Neurobiology of Stress 32 (2024) 100667

Contents lists available at ScienceDirect

Neurobiology of Stress

journal homepage: www.elsevier.com/locate/ynstr

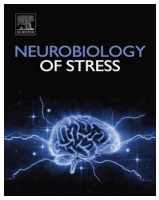

Distinct populations of lateral preoptic nucleus neurons jointly contribute to depressive-like behaviors through divergent projections in male mice

Zhiping Cao [a], Wing-Ho Yung [b,**], Ya Ke [a,*]

[a] School of Biomedical Sciences, Faculty of Medicine, The Chinese University of Hong Kong, Shatin, NT, 999077, Hong Kong, China
[b] Department of Neuroscience, Jockey Club College of Veterinary Medicine and Life Sciences, City University of Hong Kong, Kowloon Tong, Hong Kong, China

ARTICLE INFO

Handling Editor: Rita Valentino

Keywords:
Chronic restraint stress
Lateral preoptic nucleus
Lateral habenula
Ventral tegmental area
Depressive-like behaviors

ABSTRACT

The lateral preoptic area (LPO) is a component of the hypothalamus involved in various physiological functions including sleep-wakefulness transition, thermoregulation, and water-salt balance. In this study, we discovered that distinct LPO excitatory neurons project separately to the aversive processing center lateral habenula (LHb) and the reward processing hub ventral tegmental area (VTA). Following chronic restraint stress (CRS), the LHb-projecting and VTA-projecting LPO neurons exhibited increased and decreased neuronal activities, respectively. Optogenetic activation of LHb-projecting LPO excitatory neurons and LPO excitatory neuronal terminals within LHb evoked aversion and avoidance behaviors, while activation of VTA-projecting LPO excitatory neurons and LPO excitatory neuronal terminals within VTA produced preference and exploratory behaviors in mice. Furthermore, either optogenetic inhibition of LHb-projecting LPO excitatory neurons or activation of VTA-projecting LPO excitatory neurons during CRS effectively prevented the development of depressive-like behaviors. Our study unveils, for the first-time, divergent pathways originating from LPO that regulate opposite affective states in mice and implicates that an imbalance of their activities could lead to depressive-like behaviors. These circuitries represent promising therapeutic targets to relieve emotional dysfunctions in neuropsychiatric disorders.

1. Introduction

Depression is a prevalent psychiatric disorder that ranks among the top 25 leading causes of health burden worldwide according to the Global Burden of Diseases (GBD), Injuries, and Risk Factor Study in 2019 (GBD 2019 Disease and Injuries Collaborators, 2020). Epidemiological studies indicated that approximately 3.8% of the population experiences depression and nearly 280 million people in the world have depression (Malhi and Mann, 2018). Despite extensive research on brain nuclei involved in depression, such as the prefrontal cortex (Pizzagalli and Roberts, 2022), ventral tegmental area (Kaufling, 2019), hippocampus (Tartt et al., 2022), nucleus accumbens (Xu et al., 2020), and amygdala (Grogans et al., 2022), available findings for effective clinical treatments for depression remain largely insufficient. Therefore, deciphering a comprehensive circuitry responsible for the pathogenic mechanisms underlying depressive symptoms is still of great significance.

It has been documented that excitatory pyramidal neurons in the medial prefrontal cortex (mPFC) contribute significantly to depression (Jr Adams, 2009; Larsen et al., 2022). In addition, glutamatergic neurons in the ventral pallidum (VP) and substantia innominate (SI) mediate depressive-like behaviors (Luo et al., 2023; Zhang et al., 2022). Moreover, impairment of excitatory projections from various nuclei to crucial emotional centers, including lateral habenula (LHb) and ventral tegmental area (VTA), is also closely linked to the emergence of depressive-like behaviors. For instance, the increased excitation from mPFC, VP, medial septum (MS), lateral hypothalamus (LHA), entopeduncular nucleus (EPN) to LHb are intimately related to depressive-like behaviors (Zhang et al., 2022; Yang et al., 2018). At the same time, decreased glutamatergic transmission from the dorsal raphe (DRN) to VTA circuit contributes to anhedonia-like behaviors in mice (Xu et al., 2023). The lateral preoptic nucleus (LPO), an essential component of the hypothalamus, has long been known for its involvement in water-sodium regulation (Saad et al., 1996; Sessler and Salhi, 1981), locomotor control (Shreve and Uretsky, 1991), sleep homeostasis (Miracca et al., 2022; Yamagata et al., 2021), and thermoregulation (Thornhill and Halvorson, 1994). Recently, extensive research has

* Corresponding author. Lo Kwee Seong Integrated Biomedical Sciences Building, Tai Po Road, Sha Tin District, New Territories, Hong Kong, China.
** Corresponding author. Department of Neuroscience, City University of Hong Kong, Tat Chee Avenue, Kowloon, Kowloon, Hong Kong, China.
E-mail addresses: whyung@cityu.edu.hk (W.-H. Yung), yake@cuhk.edu.hk (Y. Ke).

https://doi.org/10.1016/j.ynstr.2024.100667
Received 13 May 2024; Received in revised form 6 August 2024; Accepted 7 August 2024

begun to concentrate on elucidating the role of the LPO in emotional regulation (Barker et al., 2017, 2023; Gordon-Fennell et al., 2020a, 2020b). Meanwhile, evidence from anatomical studies showed that LPO is a critical input to the LHb (Barker et al., 2017; Waung et al., 2022) and sends strong projections to the VTA (Gordon-Fennell et al., 2020a, 2020b). Notably, these LPO-recipient areas are both extensively involved in the pathology of depression (Root et al., 2014; Grace, 2016; Yang et al., 2018; Zhong et al., 2018; Kaufling, 2019; Hu et al., 2020; Morris et al., 2022). However, it remains unclear whether LPO excitatory neurons projecting to the LHb and VTA play an important role in the formation of depression.

In this study, we discovered that LPO excitatory neurons projecting to the LHb and VTA displayed opposite changes in neuronal activities following chronic restraint stress (CRS). Subsequent retrograde tracing experiments verified that LPO neurons projecting to the LHb and the VTA were distinct populations. Furthermore, optogenetic activation of LPO excitatory neurons projecting to the LHb and the VTA induced opposite behavioral performances, while optogenetic manipulation of these neurons during CRS successfully mitigated CRS-induced depressive-like behaviors. Together, these findings demonstrate, for the first time, the critical role of LPO in contributing to depressive-like behaviors through divergent downstream brain nuclei and provide a new potential therapeutic target for the clinical prevention of chronic stress-induced depression disorder.

2. Materials and methods

2.1. Animals

Adult C57/BL male mice (25–45g) were used in this study. The total number is 128 (including loss of 10 mice due to surgical complications or sub-optimal quality of brain slice preparation or wrong virus injection site or wrong placement of fibre optics). The animals were bred and maintained by the Laboratory Animal Service Centre of The Chinese University of Hong Kong (CUHK). They were group-housed in a temperature-controlled facility at 23 °C, following a regular 12-h light (8 a.m.–8 p.m.)/dark (8 p.m.–8 a.m.) cycle. All experiments were performed following the CUHK guideline approved by the Animal Experimentations and Ethics Committee.

2.2. Stereotaxic injection

Mice were anesthetized with ketamine and xylazine and placed gently in a stereotaxic frame (Narashige, Tokyo). A Hamilton syringe (33-gauge) filled with AAV viruses or chemical tracers was placed into target brain nuclei according to the corresponding stereotaxic coordinates. The coordinates for targeted brain nuclei: LPO (+0.46 mm A/P, ±0.78 mm M/L, 5.80 mm D/V), LHb (−1.47 mm A/P, ±0.48 mm M/L, 2.92 mm D/V), VTA (−2.83 mm A/P, ±0.35 mm M/L, 4.75 mm D/V) from brain skull. 0.10–0.35 μl AAV viruses or chemical tracers were injected at a speed of 10 nl/min. After completion of the injection, the needle was left in the target brain area for an additional 10 min before retraction. The following viruses and chemical tracers were used: AAV9-hSyn-ChR2-EGFP (Addgene, functional connectivity); Retro-AAV-hSyn-Cre-EGFP (Addgene, circuit-dependent neuronal labeling); AAV9-CaMKII-Dio-GCaMP6s-WPRE-hGH-polyA (BrainVTA, photometry recording); AAV9-CaMKII-ChR2-mCherry (Addgene, optogenetic activation); AAV9-CaMKII-Dio-ChR2-mCherry (BrainVTA, optogenetic activation); AAV9-CaMKII-Dio-eNpHR3.0-mCherry (BrainVTA, optogenetic inhibition); AAV9-hSyn-Dio-EGFP (Addgene, control); Cholera subunit B conjugated to AlexaFluor-488 (ThermoFisher, CTB488, retrograde tracing); Cholera subunit B conjugated to AlexaFluor-555 (ThermoFisher, CTB555, retrograde tracing). All AAV virus titers were >5 x 1012 particles per ml. The mice were allowed at least three weeks to recover before conducting behavioral tests or other experiments.

2.3. The procedure of chronic restraint stress (CRS)

As previously reported (Kim and Han, 2006), mice were restrained for 2h per day in a well-ventilated 50 ml centrifuge tube for 14 days. After CRS, the mice were subjected to depressive-like behavioral tests.

2.4. Behavioral tests

Elevated plus maze test. The self-made elevated plus maze (EPM) apparatus was made up of two open arms (25 cm [L] × 5 cm [W] × 0.5 cm [H]) and two closed arms (25 cm [L] × 5 cm [W] × 16 cm [H]) arranged in a "plus" shape and elevated 50 cm above the floor. The mice were gently placed at the junction of the open and closed arms while facing toward one of the open arms to initiate the test. Mice were allowed for a 6-min exploration. The number of entries in the open arms' zone and duration in the open arms' zone were analyzed and quantified by the ANY-Maze tracking software (Version 4.7, Stoelting CO).

Open field test. Mice were gently placed in the center of the OFT chamber (50 cm [L] × 50 cm [W] × 40 cm [H]) and allowed for free exploration for 10 min. Parameters including total distance travelled, total mobile durations, and time spent in the center zone were analyzed and quantified by the ANY-Maze tracking software (Version 4.7, Stoelting CO).

Forced swim test. The apparatus of the forced swim test was a cylindrical tank that was 30 cm high and 20 cm in diameter. And the water was 15 cm tall at room temperature (23–25 °C). Tested mice were gently put into water, and the video was recorded for 6 min. Mice's immobile time in the water was analyzed and quantified by the ANY-Maze tracking software (Version 4.7, Stoelting CO).

Sucrose preference test. Mice from different groups were habituated for two days for two bottles (one is a sucrose solution bottle, the other is a water bottle, with left and right random placement) in their home cages. After habituation, the sucrose preference of mice from both groups was tested. The intake volume of water and 2% sucrose solution were measured within 2 h. Sucrose preference was determined as the ratio of the intake volume of sucrose solution to total water consumption.

2.5. Photometry recording

Based on the above coordinates described in section **2.3**, two groups of mice were bilaterally injected with 100 nl of Retro-hSyn-Cre-EGFP into either LHb or VTA, respectively, and 200 nl of AAV9-CaMKII-Dio-GCaMP6s-WPRE-hGH-polyA into LPO of the bilateral brain. To increase the success rate, we implanted with two optic fibers 0.1–0.3 mm D/V above the targeted coordinate of LPO in the two hemispheres. Data were collected from the hemisphere with the better quality, i.e., good signal to noise ratio, stable recording, good virus expression and fiber position). Calcium signals of LHb-projecting LPO and VTA-projecting LPO excitatory neurons for each group were recorded for 5 min pre and post CRS on day 1 and day 15, respectively.

To minimize stress responses, the mice were habituated for a minimum of three days to become accustomed to the experimenters' hands prior to connecting the fiber connector. On the recording day, the mice were briefly anesthetized, and the fiber connector was carefully inserted into the fibers on their skulls. Mice were put into the cage with their bedding from their home cage for recovery from anesthetization. After experiments, mice were put back into their original home cage for normal housing. Consistency in the power of blue light was maintained throughout the entire recording process, both before and after CRS, for each individual mouse. In order to investigate the impact of the time of virus expression on changes in calcium signals, the same protocol was utilized to record the calcium activity of LHb-projecting and VTA-projecting LPO excitatory neurons from control mice.

Fiber photometry data were collected with a TDT system at a sampling frequency of 1017Hz. The LED power at the tip of the patch cord

was less than 20 μW. The 405- and 465-signals were simultaneously recorded. The isosbestic 405 nm control signal was filtered using a polyfit regression to limit the influence of fluorescence decay during the session. And the fitted control signal was then subtracted from the 465-signal to remove artifacts from the intracellular calcium-dependent GCaMP fluorescence. The calculation for the dynamics of fluorescence in chronic calcium recording was performed using the formula $\triangle F/F = (F465\text{-}F405)/F405$. As corroborated by previous studies (Xia et al., 2021; Shao et al., 2022), a calcium signal wave exceeding $\mu + 3\sigma$ was regarded as a fluorescence transient. Here, μ and σ denote the average and the standard deviation of the baseline, respectively. The baseline was randomly selected calcium recording, with a duration ranging from 5 to 10 s for each mouse. Data were visualized and analyzed with custom MATLAB scripts.

2.6. Retrograde tracing and immunostaining

For retrograde tracing, mice were unilaterally injected with 100 nL of Cholera toxin subunit B conjugated to Alexia Fluor 488 (CTB488) into LHb or 100 nL of CTB555 into VTA and allowed at least two weeks for full expression before being sacrificed. For preparations of brain samples, mice were anesthetized with i.p. injection of a ketamine-xylazine cocktail and transcardially perfused with 1X phosphate-buffered saline (PBS, Invitrogen) and then 4% paraformaldehyde (PFA, Sigma-Aldrich) using a pump at a speed of 10 mL/min. The brain was then extracted and postfixed overnight in 4% PFA and finally dehydrated with 30% glucose solution for 48h. The well-prepared brain samples were embedded in OCT (ThermoFisher) and sliced into 30-μm coronal sections by a cryostat (Leica) and stored in 1X PBS before immunohistochemistry or being mounted onto glass slides for microscopic imaging (C1, Nikon). As for the statistical analysis of CTB488 and CTB555 labeled LPO neurons, profile counting based on the Paxinos and Franklin's Mouse Brain (4th Edition) was performed on image J. For different LPO subregions, CTB488- and CTB555-positive LPO neurons on two consecutive brain slices were selected and measured. And the value averaged from the profile counting on two consecutive brain slices was regarded as the CTB488- or CTB555-positive neuronal number of the specific LPO subregion of one mouse.

For immunostaining, brain sections were blocked in PBS solution with 5% normal goat serum (ThermoFisher) and 0.3% Triton X-100 (Sigma Aldrich) for 40 min and then incubated with a cocktail of streptavidin-conjugated Alex 405 (1:1000, ThermoFisher) and primary rabbit anti-Tyrosine hydroxylase antibody (1:1000, Abcam) for VTA neurons at 4 °C overnight. After several thorough washing pieces in PBS, the sections for VTA neurons were incubated with goat anti-rabbit IgG-Alexa Fluor 555 secondary antibody (1:1000, Invitrogen) in a blocking solution for 2 h. After that, the sections were rinsed in PBS again and finally mounted onto glass slides. Microscopic images were taken under a confocal laser scanning microscope (C1, Nikon).

2.7. In vitro electrophysiology

Mice were injected with 80 nl AAV9-hSyn-ChR2-EGFP into LPO. And *in vitro* brain slice recording was performed three weeks after enough expression of the virus.

Mice quickly anesthetized by isoflurane were then transcardially perfused with pH7.4 NMDG artificial cerebrospinal fluid (aCSF) which contained (mM): NMDG 92, KCl 2.5, NaH_2PO_4 1.25, $NaHCO_3$ 20, HEPES 10, Glucose 25, Na-ascorbate 5, Thiourea 2, Na-pyruvate 3, $MgSO_4$ 10, $CaCl_2$ 0.5, N-acetyl-L-cysteine 12. Once completion of quick perfusion, the mice's brain was quickly and smoothly extracted and placed into cutting NMDG solution, where they were flash-frozen for 30s. And coronal sections at 270-μm were prepared with a vibratome (Campden 5100MZ-PLUS Vibratome) and then transferred to a chamber with 34 °C NMDG aCSF for the first 15 min of recovery. And subsequently, brain slices were further gently transferred into another chamber holding with aCSF at room temperature containing HEPES, pH 7.4, which contained (mM): NaCl 92, KCl 2.5, NaH_2PO_4 1.25, $NaHCO_3$ 20, HEPES 10, Glucose 25, Na-ascorbate 5, Thiourea 2, Na-pyruvate 3, $MgSO_4$ 10, $CaCl_2$ 0.5, N-acetyl-L-cysteine 12. After 40–60 min of recovery, the brain slice could be placed into a recording chamber with normal aCSF, pH 7.4, which contained (mM): NaCl 125, KCl 2.5, Glucose 11, $NaHCO_3$ 26, NaH_2PO_4 1.25, $CaCl_2$ 2, and $MgCl_2$ 2 for neuronal recording.

To record the optically evoked postsynaptic current, we used an internal solution containing (mM): K-gluconate 130, KCl 10, HEPES 10, EGTA 1, $MgCl_2$ 2, Na_2-ATP 2, Na_3-GTP 0.4. Light pulses at 470 nm were delivered through a light stimulator (Polygon400 DSI-E−0470-0590-NK1 Dynamic Spatial Illuminator) to activate LPO terminals while patched VTA neurons were held at −70mV. The neuron with access resistance <20 MΩ and leak current < 100 pA was included for data collection. Once completion of recording, brain slices were fixed overnight with 4% PFA. And the correct position of recorded VTA neurons were identified by staining with streptavidin-conjugated Alex 405 (ThermoFisher), while VTA TH-positive neurons were confirmed by double staining of Tyrosine hydroxylase (Abcam) and streptavidin-conjugated Alex 405 (ThermoFisher) as described above. Signals were collected using a MultiClamp 700B amplifier controlled by Clampfit 10.4 software via a Digital data 1550 interface (Molecular Devices). Electrical signals were filtered at 3 kHz, digitized at 10 kHz, and further analyzed using Clampfit 10.7 (Molecular Devices).

2.8. Optogenetic experiments

2.8.1. Optogenetic activation

For optogenetic activation of LHb-projecting or VTA-projecting LPO excitatory neurons, mice were unilaterally injected with 100 nl of Retro-hSyn-Cre-EGFP into LHb or VTA, 120 nl of AAV9-CaMKII-Dio-ChR2-mCherry into LPO and implanted with an optic fiber 0.1–0.3 mm D/V above the coordinate of LPO, followed by behavioral tests. For optogenetic activation of LPO excitatory terminals within LHb or VTA, mice were unilaterally injected with 120 nl of AAV9-CaMKII-ChR2-mCherry into LPO and implanted with optical fibers above LHb and VTA, respectively. For both LPO excitatory neuronal activation and activation of LPO excitatory terminals within LHb and VTA, real-time place preference test, elevated plus maze test, and open field test were conducted. For real-time place preference test, when mice entered the light ON chamber, 473-nm light with 10 ms, 10 Hz (Newdoon Technology) was delivered via an optic cable (200-μm core, 0.37 NA, Doric Lens) while the light was turned off when mice entered the light OFF chamber. Lights on refers to that when we visually observed a mouse entered the corresponding border of light-ON chamber, we immediately turn on the blue light. For elevated plus maze and open field tests, mice were recorded with first 3 min as the baseline, followed by second 3 min' delivery of 473-nm light stimulation with 10 ms, 10 Hz (Newdoon Technology) via an optic cable (200-μm core, 0.37 NA, Doric Lens). Laser power was 3–5 mW measured at the tip of the fiber, which was implanted 0.1–0.3 mm D/V above the coordinate of targeted nucleus.

2.8.2. Optogenetic manipulation during CRS

For optogenetic inhibition or activation during CRS, mice were bilaterally injected with 100 nl Retro-hSyn-Cre-EGFP into LHb or VTA, followed by 200 nl of AAV9-CaMKII-Dio-eNpHR3.0-mCherry or AAV9-CaMKII-Dio-ChR2-mCherry into LPO and bilaterally implanted with optic fibers 0.1–0.3 mm D/V above the coordinate of LPO. During exposure to CRS, mice LPO was simultaneously illuminated with a 589-nm light laser (Newdoon Technology) or a 478-nm light laser (Newdoon Technology) to inhibit LHb-projecting LPO or activate VTA-projecting LPO, respectively. The protocols were set at 0.0001 Hz, 9999 ms, 20 mW for LHb-projecting LPO excitatory neurons and 10 Hz, 10 ms, 10 mw for VTA-projecting LPO excitatory neurons both with a cyclical mode consisting of 3 min' light on and 3 min' light off for the whole process of CRS. The depressive-like behavioral tests were measured as

formerly mentioned and analyzed by Any-maze software.

For cohorts used in behavioral experiments, the viral injection site and the optic fiber placement were carefully confirmed as described above before inclusion in the data analysis.

2.9. Statistical analysis

Statistical analysis was performed using GraphPad Prism 8.0. The rationale for when nonparametric tests vs. One-way ANOVAs were used is correspondingly based on the unequal variances (nonparametric followed by Dunnett's test) or equal variances (One-way ANOVAs followed by Tukey post-hoc test). Equal or unequal variances were determined by the Normality and Lognormality tests. Besides, Two-way ANOVA followed by Sidak post-hoc test, Wilcoxon matched-pairs signed rank test, and unpaired Mann-Whitney test was conducted for statistical analysis. Values were shown as mean ± standard error of the mean (SEM). The value for statistical significance was $p < 0.05$.

3. Results

3.1. LHb-projecting and VTA-projecting LPO excitatory neurons exhibit opposite neuronal activities following CRS

We employed CRS to induce depressive-like behaviors in C57BL/6 mice, adopting a conventional protocol (Becker et al., 2021). To explore the potential changes of LHb-projecting and VTA-projecting LPO excitatory neuronal activities following CRS, we first prepared two batches of mice (n = 9) that allowed us to record from these neurons. We injected Retro-AAV-Cre-EGFP into the LHb and VTA respectively and injected Cre-dependent CaMKII-Dio-GCaMP6s into LPO (Fig. 1A). Before CRS, the basal depressive-like behaviors of mice and the calcium activities from the projection neurons were recorded as control. And the same protocols were applied following CRS (Fig. 1A).

Specifically, compared to the baseline behavioral performances of mice before CRS, both batches of mice exhibited decreased time spent in the open arms of the elevated plus maze (Fig. 1B, Pre *vs.* Post: LPO^{LHb}: $W = -43$, $p = 0.0078$; LPO^{VTA}: $W = -45$, $p = 0.0039$), suggesting increased anxiety levels. There were also decreased number of entries into the center of the open field (Fig. 1C, Pre *vs.* Post: LPO^{LHb}: $W = -42$, $p = 0.017$; LPO^{VTA}: $W = -45$, $p = 0.0039$), indicating decreased exploratory behaviors in mice. Importantly, in two classical tests for depression, there were decreased sucrose intake of the animals in the sucrose preference test (Fig. 1D, Pre *vs.* Post: LPO^{LHb}: $W = -37$, $p = 0.0273$; LPO^{VTA}: $W = -37$, $p = 0.0273$), indicating decreased hedonic levels of these animals, and increased immobile time in the forced swim test (Fig. 1E, Pre *vs.* Post: LPO^{LHb}: $W = 35$, $p = 0.0391$; LPO^{VTA}: $W = 43$, $p = 0.0078$), suggesting decreased levels of motivation. The data were collected only from mice with successful expression of AAV viruses within the target areas of LHb, VTA, and LPO (Fig. 1F and G).

With respect to neuronal activities, the calcium signals detected by GCaMP were typically in the form of random fluctuations superimposed with clear peaks of activities (Fig. 1H and K), which are analogous to those reported in some other studies (Xia et al., 2021; Shao et al., 2022). The detected peaks of activities surpassing set threshold (see **Materials and methods**) presumably represented short bouts of intense neuronal activities. Intriguingly, as shown by the representative traces and heatmaps from individual mice (Fig. 1H and K), we observed that LHb-projecting LPO excitatory neurons exhibited an increase in both the frequency and amplitude of the calcium transients following CRS (Fig. 1I, Pre *vs.* Post: Frequency: $W = 41$, $p = 0.0156$; Amplitude: $W = 39$, $p = 0.0195$). In contrast, the VTA-projecting LPO excitatory neurons displayed a decreased frequency and amplitude in calcium activities (Fig. 1J, Pre *vs.* Post: Frequency: $W = -45$, $p = 0.0039$; Amplitude: $W = -45$, $p = 0.0039$). These findings reveal that LHb-projecting and VTA-projecting LPO excitatory neurons were oppositely affected following CRS. In the control mice that did not undergo CRS, we did not observe significant changes in the calcium activities between day 1 and day 15 (Fig. S1), suggesting that the time of virus expression had no effect on the calcium activities and the stable recording condition in our experiments.

3.2. LHb-projecting and VTA-projecting LPO neurons are distinct populations

The previous results suggest a potential relationship between LHb-projecting/VTA-projecting LPO excitatory neurons and depressive-like behaviors following CRS. At the same time, the opposite changes of these two groups of neurons following CRS implicate the presence of different populations of neurons within LPO that project to LHb and VTA separately. To test for this notion, we unilaterally injected cholera toxin subunit B conjugated to Alexia Fluor 488 (CTB488) or 555 (CTB555) into the LHb and VTA of mice (n = 4) respectively (Fig. 2A), and quantitated the CTB488-positive, CTB555-positive as well as double-positive neurons within LPO. After recovery and confirmation of successful expression of CTB488 in LHb (Fig. 2B) and CTB555 in VTA (Fig. 2C), brain sections containing different subregions of LPO were prepared and examined under confocal microscopy. We found that LHb retrogradely-labeled LPO neurons with green fluorescence and VTA retrogradely-labeled LPO neurons with red fluorescence were comparable in quantity and had intermingled distributions within the LPO nucleus but without obvious overlap at different LPO subregions (Fig. 2D). Consistent with the findings of previous reports, we observed CTB488-positive and CTB555-positive neurons diffusely distributed at adjacent nuclei, namely the VP (Knowland et al., 2017) and hypothalamic medial preoptic area (Fang et al., 2018), respectively. At the same time, the neurons that co-expressed CTB488 and CTB555 only accounted for small percentages (2.1%) of the total CTB488- and CTB555-positive LPO neurons in different mouse brain samples (Fig. 2E). These data together confirm that the LPO neurons that project to LHb and VTA are largely distinct populations.

3.3. Activation of LHb-projecting LPO excitatory neurons and their terminals within LHb evoked aversion and anxiety-like behaviors in mice

To explore the potential relationship between the changes of these two populations of LPO excitatory neuronal activities and depressive-like behaviors following CRS, we first applied optogenetic activation of LHb-projecting LPO excitatory neurons to observe mice's emotional valence in the real-time place preference test (Fig. 3A–C). We observed that mice (n = 11) spent less time in the light-on chamber (Fig. 3D–F, test $phase_{(Baseline,\ Real\text{-}time\ place\ test,\ Post)}$ x $chamber_{(light\text{-}ON\ vs.\ light\text{-}OFF)}$: $F(2, 36) = 29.08$, $p < 0.0001$; test $phase_{(Baseline,\ Real\text{-}time\ place\ test,\ Post)}$ effect: $F(1, 36) = 18.89$, $p = 0.0001$; $chamber_{(light\text{-}ON\ vs.\ light\text{-}OFF)}$ effect: $F(2, 36) = 1.635$, $p = 0.2091$; Ligh-OFF *vs.* light-ON chamber: Baseline, $p = 0.9962$; Real-time place test, $p < 0.0001$; Post: $p = 0.6955$), suggesting that optogenetic activation of LHb-projecting LPO excitatory neurons triggers an aversive emotional valence. Notably, optogenetic activation did not affect the total locomotor activity of mice in the chambers of the real-time place preference test (Fig. 3G, Treatment $F(1.679, 20.15) = 1.829$, $p = 0.1896$; Baseline *vs.* Real-time place test: $p = 0.3773$). In the elevated plus maze, we found that mice (n = 11) exhibited both decreased time (Fig. 3I, One-way ANOVA test, Treatment $F(1.138, 11.38) = 12.58$, $p = 0.0035$; OFF *vs.* ON: $p = 0.01$) and decreased entry numbers (Fig. 3J, Treatment $F(1.604, 16.04) = 6.792$, $p = 0.0103$; OFF *vs.* ON: $p = 0.0317$) in the open arms when the LHb-projecting LPO excitatory neurons were optogenetically activated, suggesting anxiety-like behaviors and representing increased stress levels in mice. The total distance travelled was, however, unaffected (Fig. 3K, Treatment $F(1.778, 17.78) = 1.636$, $p = 0.2993$; OFF *vs.* ON: $p = 0.4521$). Finally, similar anxiety-like behaviors were observed from mice (n = 11) in the open field test when conducting optogenetic activation. When the light was on, the mice displayed decreased time (Fig. 3M, Treatment $F(1.64,$

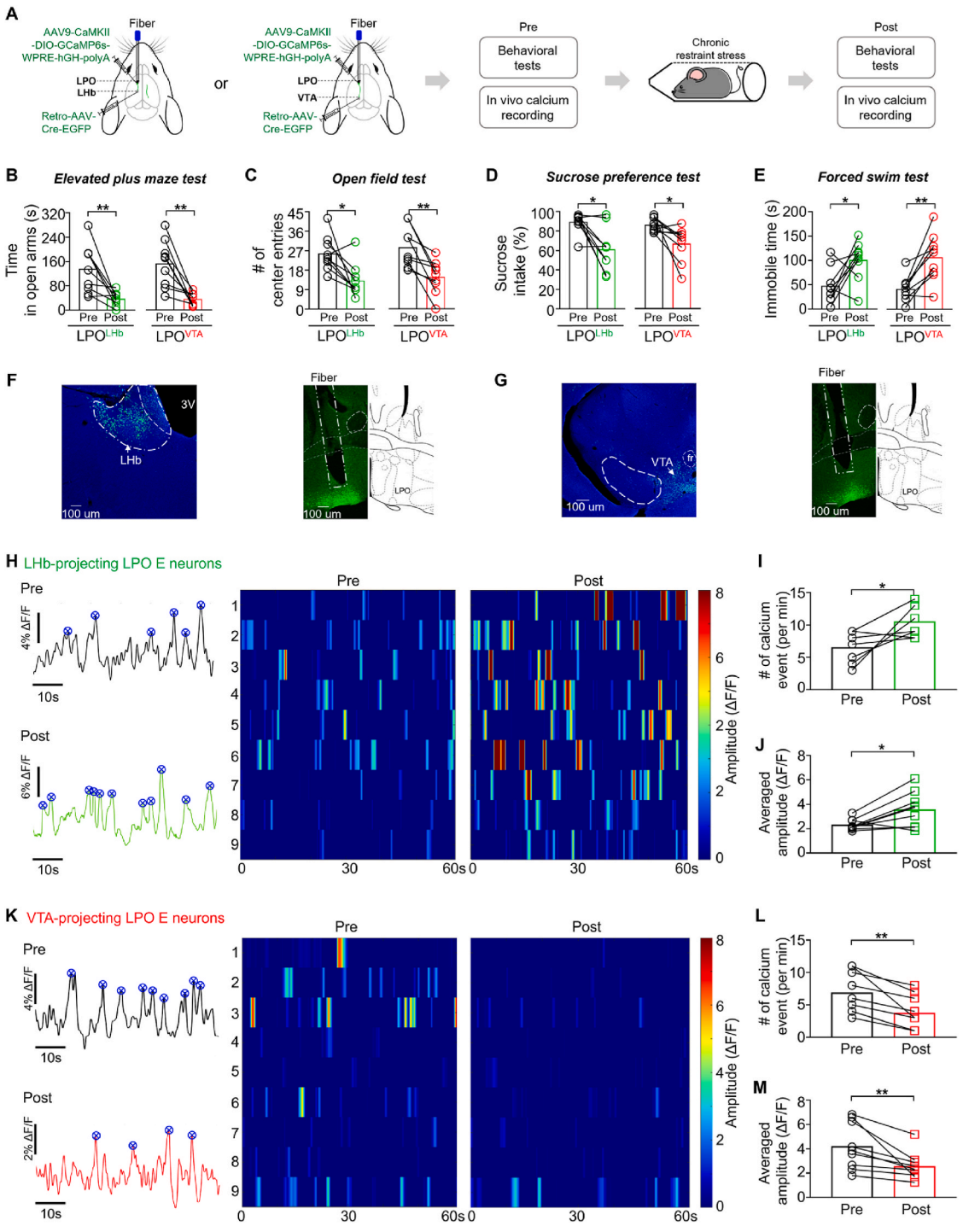

Fig. 1. LHb-projecting and VTA-projecting LPO excitatory neurons exhibited opposite neuronal activities following CRS. (A) Experimental design to determine the behavioral performance and changes of LHb-projecting and VTA-projecting LPO excitatory neuronal activities before and after building the CRS-induced depression mouse model (n = 9 mice per group). Compared to the baseline level, both groups of mice after the process of chronic restraint stress exhibited depressive-like behaviors, including **(B)** decreased time spent in open arms of the elevated plus maze (Wilcoxon matched-pairs signed rank test, LPO^{LHb}: Pre *vs.* Post: W = −43, $p = 0.0078$; LPO^{VTA}: W = −45, Pre *vs.* Post: $p = 0.0039$), **(C)** decreased number of entries into the center of the open field (Wilcoxon matched-pairs signed rank test, LPO^{LHb}: Pre *vs.* Post: W = −42, $p = 0.0117$; LPO^{VTA}: W = −45, Pre *vs.* Post: $p = 0.0039$), **(D)** decreased sucrose intake in the sucrose preference test (Wilcoxon matched-pairs signed rank test, LPO^{LHb}: Pre *vs.* Post: W = −37, $p = 0.0273$; LPO^{VTA}: Pre *vs.* Post: W = −37, $p = 0.0273$), and **(E)** increased immobile time in the forced swim test (Wilcoxon matched-pairs signed rank test, LPO^{LHb}: W = 35, Pre *vs.* Post: $p = 0.0391$; LPO^{VTA}: Pre *vs.* Post: W = 43, $p = 0.0078$). **(F, G)** Representative microphotographs showing virus expression in LHb, VTA, and LPO. **(H–J)** LHb-projecting LPO E (excitatory) neurons exhibited increased frequency (Wilcoxon matched-pairs signed rank test, W = 41, $p = 0.0156$) and amplitude (Wilcoxon matched-pairs signed rank test, W = 39, $p = 0.0195$) of calcium activities in the CRS-induced depression mouse model, each vertical stripe in the heatmap represents one calcium event for each mouse and the number 1 to 9 means 1-min's representative calcium activities each from 9 animals. **(K–M)** VTA-projecting LPO E (excitatory) neurons exhibited decreased frequency (Wilcoxon matched-pairs signed rank test, W = −45, $p = 0.0039$) and amplitude (Wilcoxon matched-pairs signed rank test, W = −45, $p = 0.0039$) of calcium activities in the CRS-induced depression mouse model. *p < 0.05, **p < 0.01, ***p < 0.001. Values are expressed as mean ± sem.

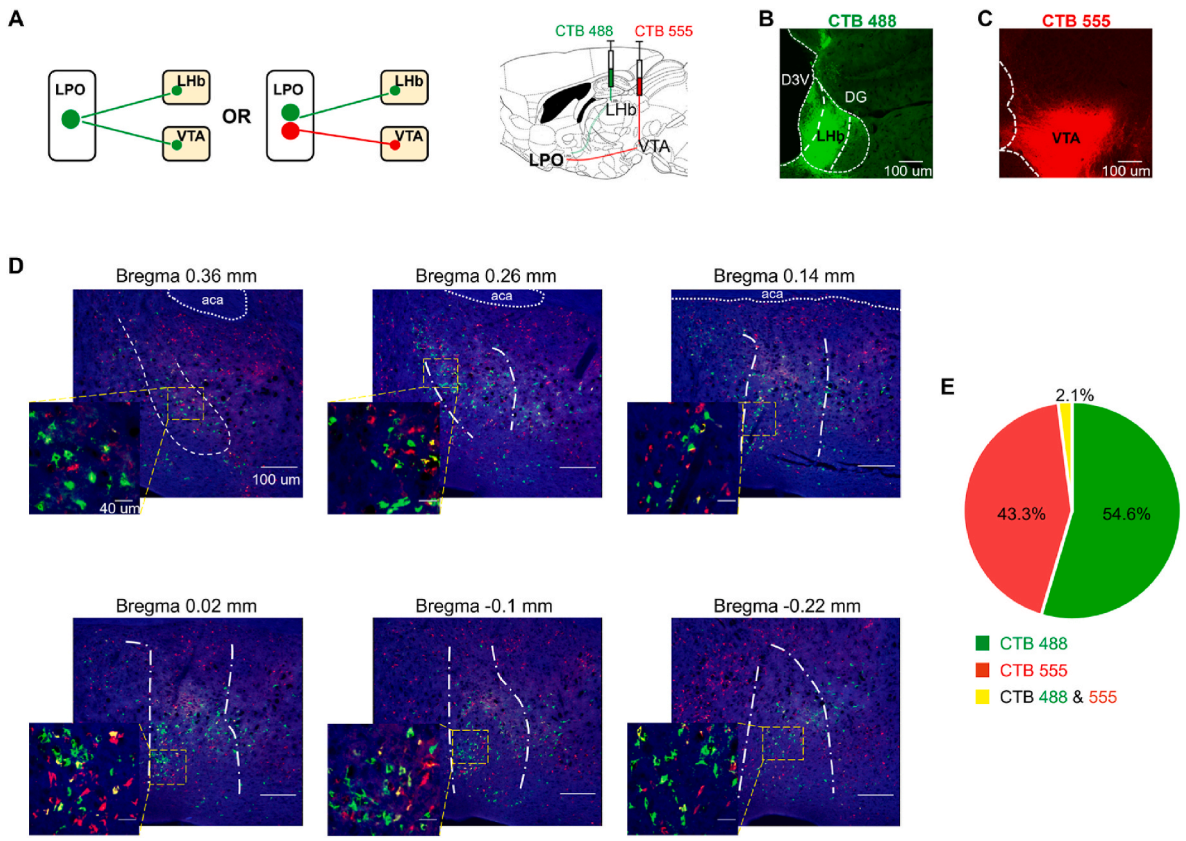

Fig. 2. LHb-projecting and VTA-projecting LPO neurons are independent populations. **(A)** Experimental design to assess the topography of LHb-projecting and VTA-projecting LPO neurons. **(B, C)** Representative microphotographs showed that CTB488 and CTB555 were successfully expressed within LHb (left) and VTA (right), respectively. Scale bar: 100 μm. **(D)** Representative microphotographs showed that retrogradely-labeled LHb-projecting (green) and VTA-projecting (red) LPO neurons with very few overlaps were observed at different sections: including bregma 0.36 mm, 0.26 mm, 0.14 mm, 0.02 mm, −0.1 mm, and −0.22 mm. Scale bar: 40 μm and 100 μm. **(E)** The distribution of LHb-projecting, VTA-projecting neurons, and their overlaps (n = 4 mice). (For interpretation of the references to colour in this figure legend, the reader is referred to the Web version of this article.)

16.4) = 0.0339, $p = 0.0339$; OFF *vs.* ON: $p = 0.0064$) in and decreased number of entries (Fig. 3N, Treatment F(1.682, 16.82) = 22.69, $p < 0.001$; OFF vs. ON: $p < 0.0001$) into the central areas of the open field, suggesting decreased risk-taking performances in mice. Again, there was no change in the total distance travelled (Fig. 3O, Treatment F(1.99, 19.9) = 0.01263, $p = 0.9872$; OFF *vs.* ON: $p = 0.987$). To further confirm our results, we also optogenetically activated the LPO excitatory terminals within the LHb (Fig. S2A). Consistently, after the light was turned on, the mice (n = 5 mice) exhibited obvious negative emotional valence in the real-time place preference test (Fig. S2D, test phase$_{(\text{Baseline, Real-time place test, Post})}$ x chamber$_{(\text{light-ON vs. light-OFF})}$: F(2, 12) = 30.53, $p < 0.0002$; test phase$_{(\text{Baseline, Real-time place test, Post})}$ effect: F(1, 12) = 41.06, $p < 0.0001$; chamber$_{(\text{light-ON vs. light-OFF})}$ effect: F(2, 12) = 4.207, $p = 0.0413$; Ligh-OFF *vs.* light-ON chamber: Baseline, $p = 0.9998$; Real-time test, $p < 0.0001$; Post: $p = 0.6306$) and anxiety-like behaviors including decreased time spent in the open arms of the elevated plus maze (Fig. S2E, nonparametric followed by Dunnett's test, $p = 0.0145$; OFF *vs.* ON: $p = 0.216$) and decreased entries into the center of the open field (Fig. S2F, nonparametric followed by Dunnett's test, $p = 0.0219$; OFF *vs.* ON: $p = 0.0415$). These results directly demonstrate that activation of LHb-projecting LPO excitatory neurons apparently show aversion and anxiety-like behaviors in mice.

3.4. *Activation of VTA-projecting LPO excitatory neurons and their terminals within VTA showed preference and risk-taking behaviors in mice*

In parallel, we investigated the effects of activating VTA-projecting LPO excitatory neurons by optogenetic strategy (Fig. 4A–C). When the light was on, as the representative trajectories in Fig. 4D and E shows, mice (n = 12) contrarily exhibited increased time spent in the light-on chamber in the real-time place preference test (Fig. 4F, test phase$_{(\text{Baseline, Real-time place test, Post})}$ x chamber$_{(\text{light-ON vs. light-OFF})}$: F(2, 33) = 36.76, $p < 0.0001$; test phase$_{(\text{Baseline, Real-time place test, Post})}$ effect: F(1, 33) = 22.72, $p < 0.0001$; chamber$_{(\text{light-ON vs. light-OFF})}$ effect: F(2, 23) = 0.0004, $p = 0.9996$; Ligh-OFF *vs.* light-ON chamber: Baseline, $p = 0.7191$; Real-time place test, $p < 0.0001$; Post: $p = 0.9343$), suggesting preference behaviors. Optogenetic activation did not affect the total locomotor activity of the animals (Fig. 4G, Baseline *vs.* Light: W = 30, $p = 0.2661$). Furthermore, the mice (n = 12) exhibited increased time (Fig. 4I, nonparametric followed by Dunnett's test, $p = 0.0024$; OFF *vs.* ON: $p = 0.0416$) and number of entries (Fig. 4J, Treatment F(1.441, 15.85) = 30.32, $p < 0.001$; OFF *vs.* ON: $p = 0.0004$) into the open arms of the elevated plus maze when the light was on, suggesting more risk-taking behaviors and representing anxiolytic effects in mice but not due to alteration in locomotion (Fig. 4K, Treatment F(1.221, 13.43) = 0.9246, $p = 0.3735$; OFF *vs.* ON: $p = 0.4205$). Consistently, in the open field test, the mice (n = 12) also showed increased time (Fig. 4M, nonparametric followed by Dunnett's test, $p = 0.0204$; OFF *vs.* ON: $p = 0.0206$) and number of entries (Fig. 4N, nonparametric followed by Dunnett's test, $p = 0.0001$; OFF *vs.* ON: $p = 0.0008$) into the center area of the arena, indicating increased risk-taking behaviors. There were also no changes in locomotor activities (Fig. 4O, nonparametric followed by Dunnett's test, $p = 0.9733$; OFF *vs.* ON: $p > 0.9999$). Furthermore, as illustrated in Fig. S3A (n = 5 mice), optogenetic activation of LPO excitatory terminals within VTA induced preference behaviors in real-time place preference test (Fig. S3D, test phase$_{(\text{Baseline, Real-time place test, Post})}$ x

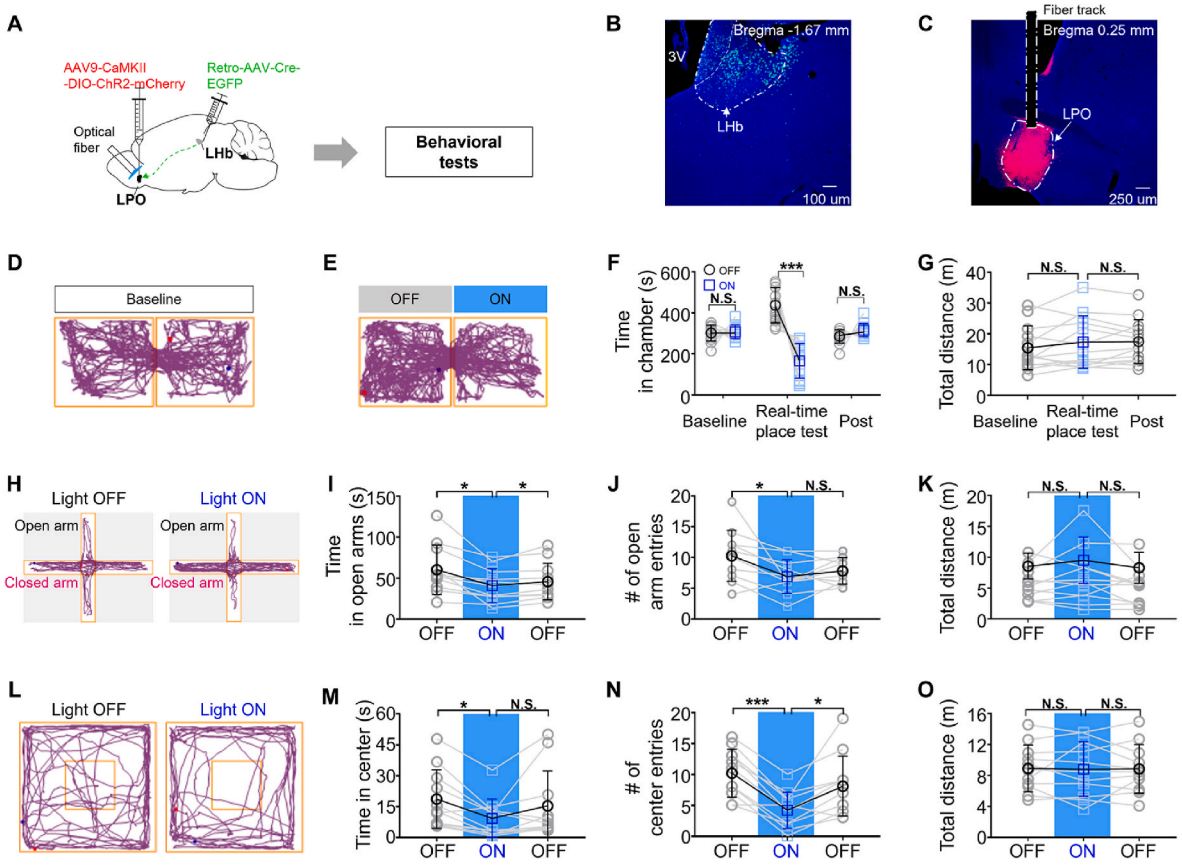

Fig. 3. Optogenetic activation of LHb-projecting LPO excitatory neurons produced aversion and anxiety-like behaviors in mice. (A) Experimental design to assess the effect of optogenetic activation of LHb-projecting LPO excitatory neurons on mice's behavioral performances. **(B, C)** Representative microphotographs showed the expression of Retro-hSyn-Cre-EGFP within LHb and AAV9-CaMKII-DIO-ChR2-mCherry in LPO. Scale bar: 100 μm and 250 μm, respectively. **(D, E)** Representative trajectories from the real-time place preference test. **(F)** Mice (n = 11) exhibited lower time in light-ON chamber (Two-way ANOVA with Sidak post-hoc test, test phase$_{(\text{Baseline, Real-time place test, Post})}$ x chamber$_{(\text{light-ON vs. light-OFF})}$: $F(2, 36) = 29.08$, $p < 0.0001$; Test phase$_{(\text{Baseline, Real-time place test, Post})}$ effect: $F(1, 36) = 18.89$, $p = 0.0001$; Chamber$_{(\text{light-ON vs. light-OFF})}$ effect: $F(2, 36) = 1.635$, $p = 0.2091$; Ligh-OFF *vs.* light-ON chamber: Baseline, $p = 0.9962$; Real-time place test, $p < 0.0001$; Post: $p = 0.6955$). **(G)** Light stimulation had no effect on locomotor activity (Wilcoxon matched-pairs signed rank test, Baseline *vs.* Real-time place test: $W = 27$, $p = 0.3757$). **(H)** Representative trajectories from the elevated plus maze test. When optogenetically activating LHb-projecting LPO excitatory neurons (a 25-s off + 10-s on + 25-s off activation strategy), mice (n = 11) exhibited **(I)** decreased time (One-way ANOVA test, Treatment $F(1.138, 11.38) = 12.58$, $p = 0.0035$; OFF *vs.* ON: $p = 0.01$; ON *vs.* OFF, $p = 0.0428$), **(J)** decreased entry numbers in the open arms (One-way ANOVA test, Treatment $F(1.604, 16.04) = 6.792$, $p = 0.0103$; OFF *vs.* ON: $p = 0.0317$; ON *vs.* OFF, $p = 0.4212$), but no effect on **(K)** locomotor activity (One-way ANOVA test, Treatment $F(1.778, 17.78) = 1.636$, $p = 0.2993$; OFF *vs.* ON: $p = 0.4521$; ON *vs.* OFF, $p = 0.2994$). **(L)** Representative trajectories from the open field test. When the light was on, mice (n = 11) displayed **(M)** decreased time (One-way ANOVA test, Treatment $F(1.64, 16.4) = 0.0339$, $p = 0.0339$; OFF *vs.* ON: $p = 0.0064$; ON *vs.* OFF, $p = 0.2238$) and **(N)** decreased center entries in the center area (One-way ANOVA test, Treatment $F(1.682, 16.82) = 22.69$, $p < 0.001$; OFF *vs.* ON: $p < 0.0001$; ON *vs.* OFF, $p = 0.012$), but no effect on **(O)** locomotor activity (One-way ANOVA test, Treatment $F(1.99, 19.9) = 0.01263$, $p = 0.9872$; ON *vs.* OFF, $p = 0.9973$). *p < 0.05, ***p < 0.001, N.S. not significant. Values are expressed as mean ± sem.

chamber$_{(\text{light-ON vs. light-OFF})}$: $F(2, 12) = 18.58$, $p = 0.0002$; test phase$_{(\text{Baseline, Real-time place test, Post})}$ effect: $F(1, 12) = 5.085$, $p = 0.0436$; chamber$_{(\text{light-ON vs. light-OFF})}$ effect: $F(2, 12) = 0.2204$, $p = 0.8054$; OFF chamber *vs.* ON chamber, Baseline, $p = 0.6623$; Real-time test, $p = 0.0001$; Post: $p = 0.5236$) and risk-taking behaviors reflected by increased time spent in the open arms of the elevated plus maze (Fig. S3E, nonparametric followed by Dunnett's test, $p = 0.0052$; OFF *vs.* ON: $p = 0.0486$) and increased numbers of entries into the center of the open field (Fig. S3F, nonparametric followed by Dunnett's test, $p = 0.0041$; OFF *vs.* ON: $p = 0.0453$).

It is well reported that VTA consists of heterogenous populations of dopaminergic and non-dopaminergic neurons (Walsh and Han, 2015; Cai and Tong, 2022). Using *in vitro* brain slice recording in combination with tyrosine hydroxylase (TH) immunostaining, we observed that TH-positive VTA neurons (n = 10 over 23 from 3 mice) mainly received excitatory projections from LPO (Fig. S4). Together, our results suggest that LPO projecting to VTA TH-positive neurons are mainly excitatory projections and optogenetic activation of VTA-projecting LPO excitatory neurons produce preference and risk-taking behaviors in mice, an effect that is opposite to that of the LHb-projecting LPO excitatory neurons.

3.5. *Contributions of LHb-projecting and VTA-projecting LPO excitatory neurons to depressive-like behaviors following CRS*

To elucidate the contributions of LHb-projecting and VTA-projecting LPO neurons to depressive-like behaviors, we applied optogenetic manipulation on these two pathways. We designed the prevention strategy based on the observation that increased activities of the LPO-LHb excitatory projection but decreased activities of LPO-VTA projection following CRS. First, for the LPO-LHb pathway, we bilaterally administered retro-AAV-Cre-EGFP into LHb and injected Cre-dependent AAV9-CaMKII-Dio-eNpHR3.0-mCherry into the LPO (Fig. 5A), which was followed by a bilateral implantation of optical fiber targeting LPO (Fig. 5B and C). Optogenetic inhibition for LHb-projecting LPO excitatory neurons was applied during the CRS procedure. This strategy could largely prevent CRS-induced depressive-like behaviors. Thus,

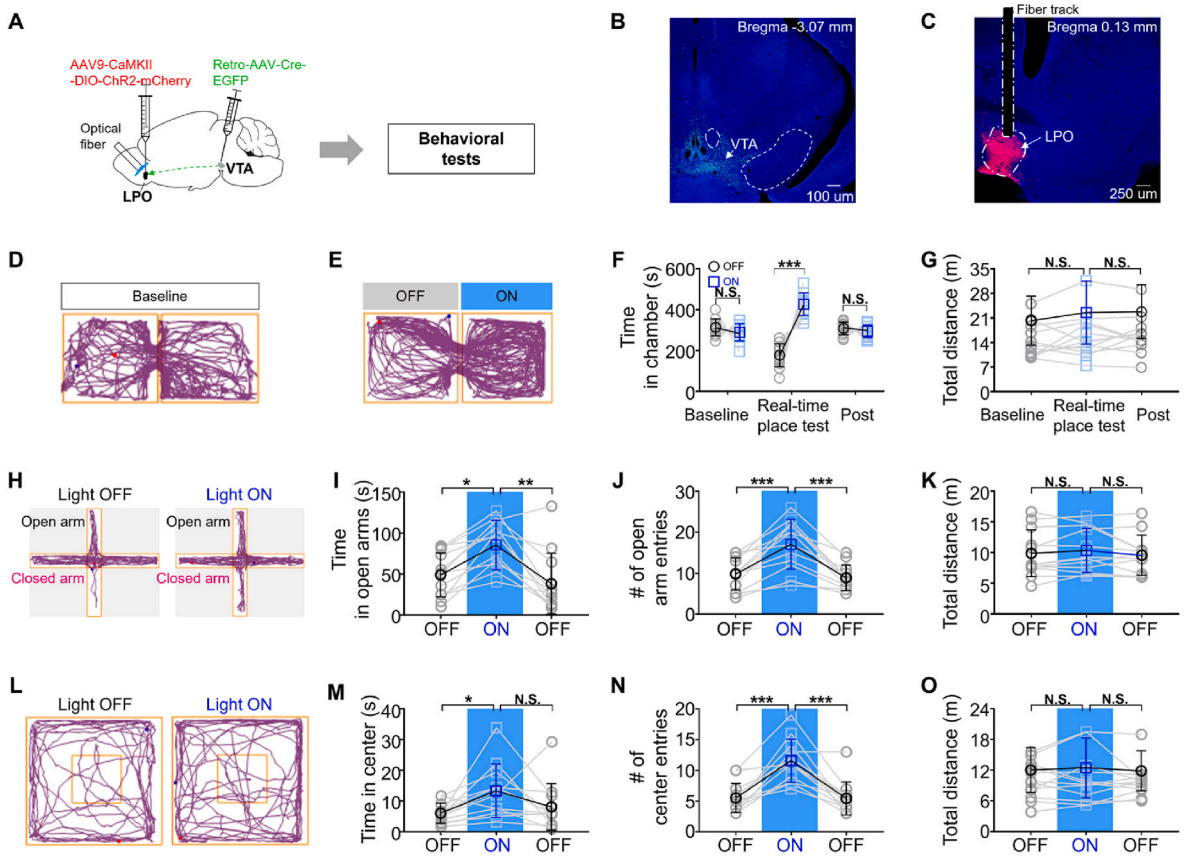

Fig. 4. Optogenetic activation of VTA-projecting LPO excitatory neurons produced preference and risk-taking behaviors in mice. (A) Experimental design to assess the effect of optogenetic activation of VTA-projecting LPO excitatory neurons on mice's behavioral performances. **(B, C)** Representative microphotographs showed the expression of Retro-hSyn-Cre-EGFP within VTA and AAV9-CaMKII-DIO-ChR2-mCherry in LPO. Scale bar: 250 μm. **(D, E)** Representative trajectories from the real-time place preference test. **(F)** Mice (n = 12) exhibited more time in light-ON chamber (Two-way ANOVA with Sidak post-hoc test, test phase$_{(\text{Baseline, Real-time place test, Post})}$ x chamber$_{(\text{light-ON vs. light-OFF})}$: $F(2, 33) = 36.76$, $p < 0.0001$; test phase$_{(\text{Baseline, Real-time place test, Post})}$ effect: $F(1, 33) = 22.72$, $p < 0.0001$; chamber$_{(\text{light-ON vs. light-OFF})}$ effect: $F(2, 23) = 0.0004$, $p = 0.9996$; Ligh-OFF *vs.* light-ON chamber: Baseline, $p = 0.7191$; Real-time place test, $p < 0.0001$; Post: $p = 0.9343$), and **(G)** light stimulation had no effect on locomotor activity (Wilcoxon matched-pairs signed rank test, Baseline *vs.* Real-time place test: $W = 30$, $p = 0.2661$). **(H)** Representative trajectories from the elevated plus maze test. When optogenetically activating VTA-projecting LPO excitatory neurons (a 25-s off + 10-s on + 25-s off activation strategy), mice (n = 12) exhibited **(I)** increased time (nonparametric followed by Dunnett's test, $p = 0.0024$; OFF *vs.* ON: $p = 0.0416$; ON *vs.* OFF, $p = 0.0024$), **(J)** increased entry numbers in the open arms (One-way ANOVA test, Treatment $F(1.441, 15.85) = 30.32$, $p < 0.001$; OFF *vs.* ON: $p = 0.0004$; ON *vs.* OFF, $p = 0.0002$), but no effect on **(K)** locomotor activity (One-way ANOVA test, Treatment $F(1.221, 13.43) = 0.9246$, $p = 0.3735$; OFF *vs.* ON: $p = 0.4205$; ON *vs.* OFF, $p = 0.3516$). **(L)** Representative trajectories from the open field test. When the light was on, mice (n = 12) displayed **(M)** increased time (nonparametric followed by Dunnett's test, $p = 0.0204$; OFF *vs.* ON: $p = 0.0206$; ON *vs.* OFF, $p = 0.1542$), **(N)** increased center entries in the center area (nonparametric followed by Dunnett's test, $p = 0.0001$; OFF *vs.* ON: $p = 0.0008$; ON *vs.* OFF, $p = 0.0005$), but no effect on **(O)** locomotor activity (nonparametric followed by Dunnett's test, $p = 0.9733$; OFF *vs.* ON: $p > 0.9999$; ON *vs.* OFF, $p > 0.9999$). *p < 0.05, **p < 0.01, ***p < 0.001, N.S. not significant. Values are expressed as mean ± sem.

compared with the CRS alone group, the mice from CRS + inhibition group (n = 8) exhibited improved anxiety-like behaviors including more time (Fig. 5D, Treatment $F(2, 33) = 11.22$, $p = 0.0002$; CRS vs. CRS + inhibition, $p = 0.0056$) and increased number of entries into the open arms of the elevated plus maze (Fig. 5E, Treatment $F(2, 33) = 6.542$, $p = 0.004$; CRS vs. CRS + inhibition, $p = 0.0056$), suggesting relieved anxiety levels, and an increased time spent in the center of the open field (Fig. 5F, Treatment $F(2, 33) = 14.49$, $p < 0.001$; CRS vs. CRS + inhibition, p = 0.0056) despite no changes in the number of entries (Fig. 5G, Treatment $F(2, 33) = 17.98$, $p < 0.0001$; CRS vs. CRS + inhibition, $p = 0.466$), suggesting improved risk-taking performances. Additionally, mice exhibited increased sucrose consumption (Fig. 5H, Treatment $F(2, 33) = 5.825$, $p = 0.0068$; CRS vs. CRS + inhibition, $p = 0.0109$), representing decreased anhedonia performances, and decreased immobile time (Fig. 5I, Treatment $F(2, 33) = 4.406$, $p = 0.0201$; CRS vs. CRS + inhibition, $p = 0.039$) in the forced swim test, suggesting decreased passive coping behaviors.

In parallel, for the LPO-VTA pathway, we bilaterally administered retro-AAV-Cre-EGFP into VTA and injected AAV9-CaMKII-Dio-ChR2-mCherry into the LPO (Fig. 5J and K), followed by a bilateral implantation of optical fiber targeting LPO (Fig. 5L). After optogenetic activation of VTA-projecting LPO excitatory neurons during CRS procedure, mice (n = 9) also exhibited reduced anxiety-like behaviors including increased time (Fig. 5M, Treatment $F(2, 34) = 7.561$, $p = 0.0019$; CRS *vs.* CRS + activation, $p = 0.0021$) and number of entries in the open arms of the elevated plus maze (Fig. 5N, Treatment $F(2, 34) = 12.07$, $p = 0.0001$; CRS *vs.* CRS + activation, $p = 0.0001$), increased number of entries into (Fig. 5O, Treatment $F(2, 34) = 3.343$, $p = 0.0473$; CRS *vs.* CRS + activation, $p = 0.3130$), and increased time spent in the center (Fig. 5P, Treatment $F(2, 34) = 4.52$, $p = 0.0182$; CRS *vs.* CRS + activation, $p = 0.0317$) in the open field test. There were also increased sucrose intake in the sucrose preference test (Fig. 5Q, Treatment $F(2, 34) = 7.217$, $p = 0.0024$; CRS *vs.* CRS + activation, $p = 0.0363$) and decreased immobile time in the forced swim test (Fig. 5R, Treatment $F(2, 34) = 14.01$, $p < 0.0001$; CRS *vs.* CRS + activation, $p = 0.0112$). These results collectively confirm the contributions of both LHb-projecting and VTA-projecting LPO excitatory neurons to CRS-induced depressive-like behaviors.

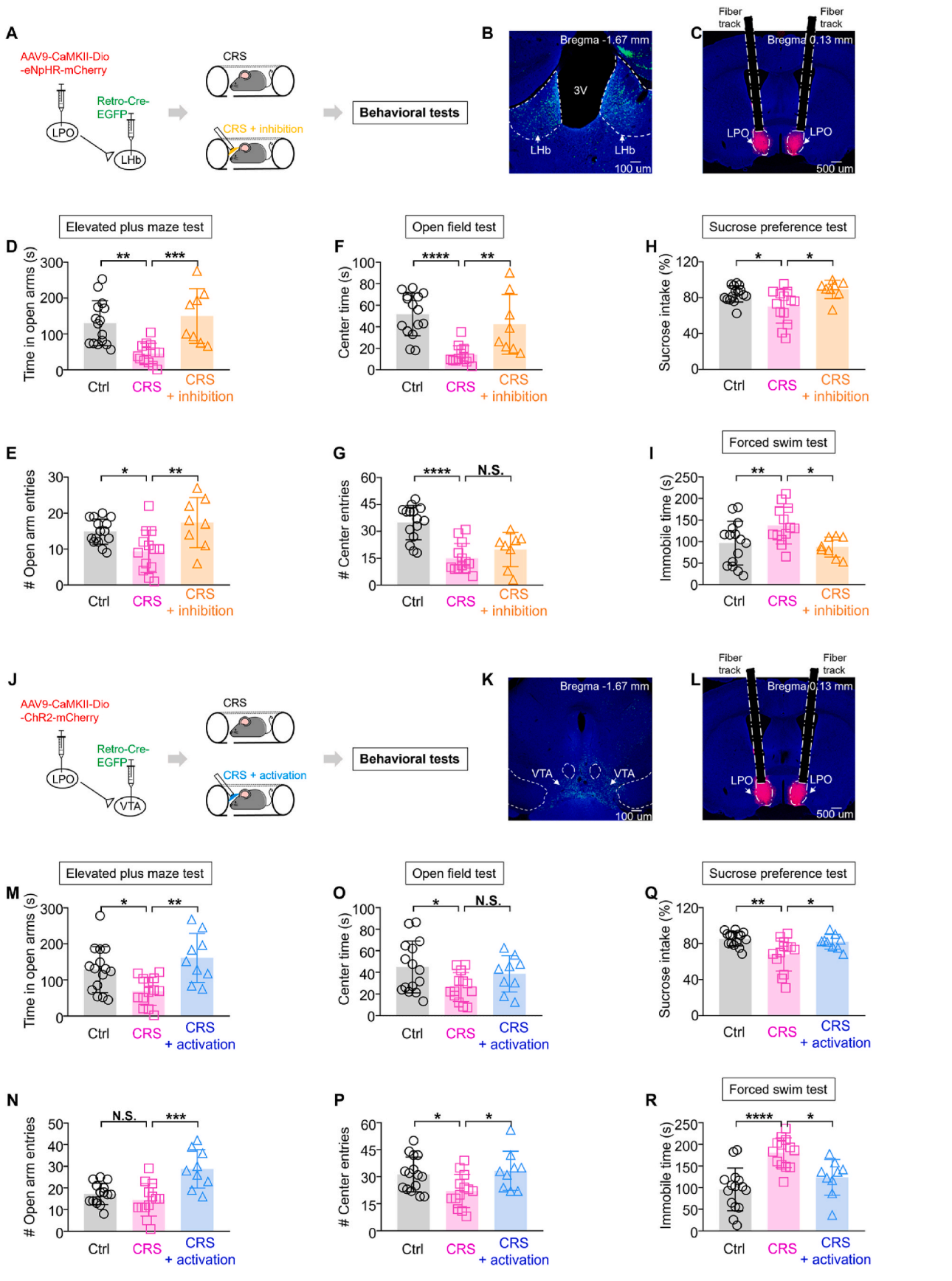

(caption on next page)

Fig. 5. Optogenetic inhibition of LHb-projecting or activation of VTA-projecting LPO excitatory neurons during chronic restraint stress prevented depressive-like behaviors in mice. **(A)** Experimental design to assess the effect of optogenetic inhibition of LHb-projecting LPO excitatory neurons during chronic restraint stress on depressive-like behaviors in the CRS-induced depression mouse model. **(B, C)** Representative virus expression in the LHb and LPO. Using a 3-min off + 3-min on + 3-min off optogenetic stimulation paradigm, mice (n = 15 for control group, n = 13 for CRS group, and n = 8 for CRS + inhibition group) throughout optogenetic inhibition during chronic restraint stress displayed **(D)** increased time spent in open arms (One-way ANOVA test with Tukey post-hoc test, Treatment $F(2, 23) = 11.22$, $p = 0.0002$; Ctrl *vs.* CRS: $p = 0.0011$; CRS *vs.* CRS + inhibition, $p = 0.0007$) and **(E)** increased number of entries into open arms in the elevated plus maze test (One-way ANOVA test with Tukey post-hoc test, Treatment $F(2, 33) = 6.542$, $p = 0.004$; Ctrl *vs.* CRS: $p < 0.0001$; CRS *vs.* CRS + inhibition, $p = 0.0056$), **(F)** increased center time (One-way ANOVA test with Tukey post-hoc test, Treatment $F(2, 33) = 14.49$, $p < 0.001$; Ctrl *vs.* CRS: $p < 0.001$; CRS *vs.* CRS + inhibition, $p = 0.0056$) but no effect on **(G)** number of entries in the center in the open field test (One-way ANOVA test with Tukey post-hoc test, Treatment $F(2, 33) = 17.98$, $p < 0.0001$; Ctrl *vs.* CRS: $p < 0.0001$; CRS *vs.* CRS + inhibition, $p = 0.466$). And **(H)** increased percentage of sucrose intake in sucrose preference test (One-way ANOVA test with Tukey post-hoc test, Treatment $F(2, 33) = 5.825$, $p = 0.0068$; Ctrl *vs.* CRS: $p = 0.0297$; CRS *vs.* CRS + inhibition, $p = 0.0109$) while **(I)** decreased immobile time in forced swim test (One-way ANOVA test with Tukey post-hoc test, Treatment $F(2, 33) = 4.406$, $p = 0.0201$; Ctrl *vs.* CRS: $p = 0.0459$; CRS *vs.* CRS + inhibition, $p = 0.039$). **(J)** Experimental design to assess the effect of optogenetic activation of VTA-projecting LPO excitatory neurons during chronic restraint stress on depressive-like behaviors in the CRS-induced depression mouse model. **(K, L)** Representative virus expression in VTA and LPO. Mice (n = 15 for control group, n = 13 for CRS group, and n = 9 for CRS + activation group) after optogenetic activation during chronic restraint stress displayed **(M)** increased time spent in open arms (One-way ANOVA test with Tukey post-hoc test, Treatment $F(2, 34) = 7.561$, $p = 0.0019$; Ctrl *vs.* CRS: $p = 0.0242$; CRS *vs.* CRS + activation, $p = 0.0021$) and **(N)** increased number of entries into open arms in the elevated plus maze test (One-way ANOVA test with Tukey post-hoc test, Treatment $F(2, 34) = 12.07$, $p = 0.0001$; Ctrl *vs.* CRS: $p = 0.5592$; CRS *vs.* CRS + activation, $p = 0.0001$), **(O)** no effect on the time in the center (One-way ANOVA test with Tukey post-hoc test, Treatment $F(2, 34) = 3.343$, $p = 0.0473$; Ctrl *vs.* CRS: $p = 0.0385$; CRS *vs.* CRS + activation, $p = 0.313$) but **(P)** increased number of entries in the center in the open field test (One-way ANOVA test with Tukey post-hoc test, Treatment $F(2, 34) = 4.52$, $p = 0.0182$; Ctrl *vs.* CRS: $p = 0.0453$; CRS *vs.* CRS + activation, $p = 0.0317$). And **(Q)** increased percentage of sucrose intake in sucrose preference test (One-way ANOVA test with Tukey post-hoc test, Treatment $F(2, 34) = 7.217$, $p = 0.0024$; Ctrl *vs.* CRS: $p = 0.0023$; CRS *vs.* CRS + activation, $p = 0.0363$) while **(R)** decreased immobile time in forced swim test (One-way ANOVA test with Tukey post-hoc test, Treatment $F(2, 34) = 14.01$, $p < 0.0001$; Ctrl *vs.* CRS: $p < 0.0001$; CRS *vs.* CRS + activation, $p = 0.0112$). *p < 0.05, **p < 0.01, ***p < 0.001, N.S. not significant. Values are expressed as mean ± sem.

4. Discussion

Despite the surging interest in the role of LPO in emotional regulation, less attention has been paid to understanding how LPO is involved in emotional dysfunctions such as depressive-like behaviors. In this study, not only that we discovered two distinct populations of LPO excitatory neurons that separately target LHb and VTA, intriguingly, we observed that these divergent pathways are modulated in an opposite manner following CRS that leads to depressive-like behaviors in male mice. Optogenetic activation of these two pathways results in opposite affective states and strategic manipulation could effectively prevent CRS-induced depressive-like behaviors. Therefore, these findings enrich our understanding of the potential brain regions involved in the formation of depressive-like behaviors and further demonstrate the potential function of LPO in emotional regulation.

Accumulated evidence suggested direct connections between LPO to LHb and LPO to VTA (Barker et al., 2017; Gordon-Fennell et al., 2020a, 2020b; Zheng et al., 2022). Our results further demonstrated LHb-projecting LPO and VTA-projecting LPO neurons are two independent populations. Meanwhile, previous reports provided some insights into the nature of connectivity between LPO to LHb and LPO to VTA. For instance, Barker et al. (2017) emphasized that a significant proportion of LPO excitatory and inhibitory neurons project to the same LHb neuron. For the LPO to VTA connection, Gordon-Fennell et al. (2020b) reported a predominance of LPO inhibitory neurons projecting to the VTA. However, another study suggested comparable levels of GABAergic and glutamatergic LPO neurons projecting to the VTA (Kalló et al., 2015). In our study, using *in vitro* electrophysiology in combination with TH-immunostaining within VTA, we revealed that the projections from LPO to VTA TH-positive neurons are mainly excitatory connections. The potential reason behind these different results may lie in the different experimental methods applied. For example, studies from Gordon-Fennell et al. (2020b) and Kalló et al. (2015) mainly clarified the type of projections by using *in situ* fluorescent hybridization and immunohistochemistry, respectively, while we adopted the ex vivo electrophysiological recording. In addition, VTA is anatomically and functionally classified into different subregions (Pistillo et al., 2015). Gordon-Fennell et al. (2020b) mainly focused on the mid-rostral and mid-caudal VTA regions. And Kalló et al. (2015) also targeted specific subregions of VTA. In our study, we randomly patched the neurons among different subregions of VTA. Such a nuance of the working area within VTA in our study compared with others may also make our results different from others. The elucidation of the detailed connections between the LPO and VTA warrants further study.

In terms of emotional function, consistent with other reports (Barker et al., 2017; Zheng et al., 2022), optogenetic activation of LHb-projecting LPO excitatory neurons and LPO excitatory terminals within LHb produced aversion and avoidance behaviors in mice. However, our study differed from previous research regarding the effects of activating LPO to VTA circuit, which induced real-time place preference in our experiments but aversion in others reports (e.g. Gordon-Fennell et al., 2020b). Given the possible heterogeneity of LPO neurons in targeting different downstream neuronal populations, the discrepancy may lie in the specific neuronal subtypes targeted within LPO, as we made use of CaMKII promotor-dominated ChR2 instead of hSyn promotor-triggered ChR2.

LPO neurons were previously reported to exhibit increased calcium activities in response to aversive stimuli (Gordon-Fennell et al., 2020b; Zheng et al., 2022). Furthermore, there was direct evidence which showed that LPO glutamatergic projections to LHb mediated aversive emotional valence (Barker et al., 2017). Thus, our results are consistent with these previous findings with respect to the LPO to LHb pathway. Different from this connection, VTA-projecting LPO excitatory neurons displayed decreased activities in the CRS-induced depressive-like behaviors. Numerous reports had demonstrated that the dopaminergic neurons in VTA played an important role in the pathology of depressive-like behaviors (Grace, 2016; Root et al., 2014; Zhong et al., 2018). Earlier reports also suggested a function of the LPO-VTA connection in motivation (e.g. Gordon-Fennell et al., 2020a). Our results demonstrated that optogenetic activation of LPO excitatory projections to VTA produced a real-time place preference and risk-taking behaviors in both the elevated plus maze and open field, suggesting that the decreased calcium activities observed in the CRS-induced depressive-like behaviors may signify decreased motivation.

LPO was reported receiving inputs from different emotion centers, such as ventral hippocampus (Cenquizca and Swanson, 2006), dorsal raphe (Zhou et al., 2017) and locus coeruleus (Saito et al., 2018). In terms of mechanism, potentiation in synaptic plasticity has been suggested to underlie chronic stress-induced depressive-like behaviors, e.g. in the neural circuits from lateral hypothalamus to LHb and from the entopeduncular nucleus to LHb (Zheng et al., 2022; Shabel et al., 2013). We thus speculate that LPO might assimilate different information from various emotion centers to contribute to the depressive-like behaviors through its projections to LHb and VTA, a hypothesis that should be

tested in the future. Notably, the intermingled distributions of LHb-projecting and VTA-projecting LPO excitatory neurons implicate an interacting network with balancing opposite forces and these two pathways may interact in some way to contribute to the observed depressive-like behaviors. This was further confirmed through our optogenetic manipulation of either LHb-projecting or VTA-projecting LPO excitatory neurons during the process of chronic restraint stress, which successfully prevented depressive-like behaviors in mice. These results suggest that activity of LPO to LHb projections is required to develop these depressive-like behaviors following CRS and stimulation of LPO to VTA projections during CRS can block the development of depressive-like behaviors. As artificial means of activation and inhibition, the optogenetic manipulations may not recapitulate the physiological changes in firing rates or patterns of LPO neurons induced by CRS. Overall, however, our data converge to support the essential roles LPO-LHb or LPO-VTA in the establishment of CRS-induced depressive-like behaviors.

Our study provides the first evidence that the LPO, one of the major subregions of the hypothalamus, is involved in the generation of depressive-like behaviors through specific population of neurons. The effect of fluctuating ovarian hormones on behavioral performance was an important consideration in our decision to conduct the study exclusively on male mice. Despite this, our findings on male mice may be pertinent to female mice. Moreover, despite the findings of this study, the specific sources innervating two populations of LPO excitatory neurons require further investigation. It is also of great interest to explore whether the present findings can be verified in other chronic stress protocols, such as social defeat exposure, social isolation, and chronic mild stressors (Cryan and Mombereau, 2004). And it would be important to elucidate the significance of LPO inhibitory neurons in emotional regulation.

In conclusion, our study unveiled divergent circuits originating from the hypothalamic LPO with opposite influences on affective valence and behavioral performances. A loss of balance between these two circuitries may contribute to CRS-induced depressive-like behaviors. These findings shed light on the intricate circuitry underlying depressive-like behaviors and provide new potential targets for therapeutic prevention.

Data sharing statement

All the data from our study are shown in the manuscript and supplemental materials are available from the corresponding author upon reasonable request.

CRediT authorship contribution statement

Zhiping Cao: Writing – review & editing, Writing – original draft, Methodology, Investigation, Formal analysis, Data curation. **Wing-Ho Yung:** Writing – review & editing, Writing – original draft, Supervision, Resources, Investigation, Funding acquisition, Conceptualization, Project administration. **Ya Ke:** Writing – review & editing, Supervision, Resources, Investigation, Funding acquisition, Conceptualization, Project administration.

Declaration of competing interest

Authors have no conflicts of interests to report.

Data availability

Data will be made available on request.

Acknowledgements

This work was supported by HKRGC-CRF grants C4012-22G, C6034-21G, HKRGC-GRF grants 14112523, 14113522 and HMRF grant 09203236.

Appendix A. Supplementary data

Supplementary data to this article can be found online at https://doi.org/10.1016/j.ynstr.2024.100667.

References

Barker, D.J., Miranda-Barrientos, J.M., Zhang, S.L., Root, D.H., Wang, H.L., Liu, B., et al., 2017. Lateral preoptic control of the lateral habenula through convergent glutamate and GABA transmission. Cell Rep. 21, 1757–1769. https://doi.org/10.1016/j.celrep.2017.10.066.

Barker, D.J., Zhang, S.L., Wang, H.L., Estrin, D.J., Miranda-Barrientos, J., Liu, B., et al., 2023. Lateral preoptic area glutamate neurons relay nociceptive information to the ventral tegmental area. Cell Rep. 42, 113029 https://doi.org/10.1016/j.celrep.2023.113029.

Becker, M., Pinhasov, A., Ornoy, A., 2021. Animal models of depression: what can they teach us about the human disease? Diagnostics 11, 123. https://doi.org/10.3390/diagnostics11010123.

Cai, J., Tong, Q.C., 2022. Anatomy and function of ventral tegmental area glutamate neurons. Front. Neural Circ. 16, 867053 https://doi.org/10.3389/fncir.2022.867053.

Cenquizca, L.A., Swanson, L.W., 2006. An analysis of direct hippocampal cortical field CA1 axonal projections to diencephalon in the rat. J. Comp. Neurol. 497, 101–114. https://doi.org/10.1002/cne.20985.

Cryan, J.F., Mombereau, C., 2004. In search of a depressed mouse: utility of models for studying depression-related behavior in genetically modified mice. Mol. Psychiatr. 9, 324–357. https://doi.org/10.1038/sj.mp.4001457.

Fang, Y.Y., Yamaguchi, T., Song, S.C., Tritsch, N.X., Lin, D.Y., 2018. A hypothalamic midbrain pathway essential for driving maternal behaviors. Neuron 98, 192–207. https://doi.org/10.1016/j.neuron.2018.02.019.

GBD 2019 Disease and Injuries Collaborators, 2020. Global burden of 369 diseases and injuries in 204 countries and territories, 1990-2019: a systematic analysis for the Global Burden of Disease Study 2019. Lancet 396, 1204–1222. https://doi.org/10.1016/S0140-6736(20)30925-9.

Gordon-Fennell, A.G., Will, R.G., Ramachandra, V., Gordon-Fennell, L., Dominguez, J. M., Zahm, D.S., Marinelli, M., 2020a. The lateral preoptic area: a novel regulator of reward seeking and neuronal activity in the ventral tegmental area. Front. Neurosci. 13, 1433. https://doi.org/10.3389/fnins.2019.01433.

Gordon-Fennell, A.G., Gordon-Fennell, L., Desaivre, S., Marinelli, M., 2020b. The lateral preoptic area and its projection to the VTA regulate VTA activity and drive complex reward behaviors. Front. Syst. Neurosci. 14, 581830 https://doi.org/10.3389/fnsys.2020.581830.

Grace, A.A., 2016. Dysregulation of the dopamine system in the pathophysiology of schizophrenia and depression. Nat. Rev. Neurosci. 17, 524–532. https://doi.org/10.1038/nrn.2016.57.

Grogans, S.E., Fox, A.S., Shackman, A.J., 2022. The amygdala and depression: a sober reconsideration. Am. J. Psychiatr. 179, 454–457. https://doi.org/10.1176/appi.ajp.20220412.

Hu, H.L., Cui, Y.H., Yang, Y., 2020. Circuits and functions of the lateral habenula in health and in disease. Nat. Rev. Neurosci. 21, 277–295. https://doi.org/10.1038/s41583-020-0292-4.

Jr Adams, J.D., 2009. Chemical interactions with pyramidal neurons in layer 5 of the cerebral cortex: control of pain and anxiety. Curr. Med. Chem. 16, 3476–3479. https://doi.org/10.2174/092986709789057626.

Kalló, I., Molnár, C.S., Szöke, S., Fekete, C., Hrabovszky, E., Liposits, Z., 2015. Area-specific analysis of the distribution of hypothalamic neurons projecting to the rat ventral tegmental area, with special reference to the GABAergic and glutamatergic efferents. Front. Neuroanat. 9, 112. https://doi.org/10.3389/fnana.2015.00112.

Kaufling, J., 2019. Alterations and adaptation of ventral tegmental area dopaminergic neurons in animal models of depression. Cell Tissue Res. 377, 59–71. https://doi.org/10.1007/s00441-019-03007-9.

Kim, K.S., Han, P.L., 2006. Optimization of chronic stress paradigms using anxiety- and depression-like behavioural parameters. J. Neurosci. Res. 83, 497–507. https://doi.org/10.1002/jnr.20754.

Knowland, D., Lilascharoen, V., Pacia, C.P., Shin, S., Wang, E.H.J., Lim, B.K., 2017. Distinct ventral pallidal neural populations mediate separate symptoms of depression. Cell 170, 284–297. https://doi.org/10.1016/j.cell.2017.06.015.

Larsen, N.Y., Vihrs, N., Møller, J., Sporring, J., Tan, X.K., et al., 2022. Layer III pyramidal cells in the prefrontal cortex reveal morphological changes in subjects with depression, schizophrenia, and suicide. Transl. Psychiatry 12, 363. https://doi.org/10.1038/s41398-022-02128-0.

Luo, Y.J., Ge, Jing, Chen, Z.K., Liu, Z.L., Lazarus, M., Qu, W.M., et al., 2023. Ventral pallidal glutamatergic neurons regulate wakefulness and emotion through separated projections. iScience 26, 107385. https://doi.org/10.1016/j.isci.2023.107385.

Malhi, G.S., Mann, J.J., 2018. Depression. Lancet 392, 2299–2312. https://doi.org/10.1016/S0140-6736(18)31948-2.

Miracca, G., Anuncibay-Soto, B., Tossell, K., Yustos, R., Vyssotski, A.L., Franks, N.P., Wisden, W., 2022. NMDA receptors in the lateral preoptic hypothalamus are essential for sustaining NREM and REM sleep. J. Neurosci. 42, 5389–5409. https://doi.org/10.1523/JNEUROSCI.0350-21.2022.

Morris, L.S., Mehta, M., Ahn, C., Corniquel, M., Verma, G., Delman, B., Hof, P.R., Jacob, Y., Balchandani, P., Murrough, J.W., 2022. Ventral tegmental area integrity measured with high-resolution 7-Tesla MRI relates to motivation across depression and anxiety diagnoses. Neuroimage 264, 119704. https://doi.org/10.1016/j.neuroimage.2022.119704.

Pizzagalli, D.A., Roberts, A.C., 2022. Prefrontal cortex and depression. Neuropsychopharmacology 47, 225–246. https://doi.org/10.1038/s41386-021-01160-w.

Pistillo, F., Clementi, F., Zoli, M., Gotti, C., 2015. Nicotinic, glutamatergic and dopaminergic synaptic transmission and plasticity in the mesocorticolimbic system: focus on nicotine effects. Prog. Neurobiol. 124, 1–27. https://doi.org/10.1016/j.pneurobio.2014.10.002.

Root, D.H., Mejias-Aponte, C.A., Zhang, S.L., Wang, H.L., Hoffman, A.F., Lupica, C.R., Morales, M., 2014. Single rodent mesohabenular axons release glutamate and GABA. Nat. Neurosci. 17, 1543–1551. https://doi.org/10.1038/nn.3823.

Saito, Y.C., Maejima, T., Nishitani, M., Hasegawa, E., Yanagawa, Y., Mieda, M., Sakurai, T., 2018. Monoamines inhibit GABAergic neurons in ventrolateral preoptic area that make direct synaptic connections to hypothalamic arousal neurons. J. Neurosci. 38, 6366–6378. https://doi.org/10.1523/JNEUROSCI.2835-17.2018.

Saad, W.A., Luiz, A.C., De Arruda Camargo, L.A., Renzi, A., Manani, J.V., 1996. The lateral preoptic area plays a dual role in the regulation of thirst in the rat. Brain Res. Bull. 39, 171–176. https://doi.org/10.1016/0361-9230(95)02089-6.

Sessler, F.M., Salhi, M.D., 1981. Interaction of hypertonic NaCl solution and neural stimuli on lateral preoptic neurons. Neurosci. Lett. 26, 319–324. https://doi.org/10.1016/0304-3940(81)90152-X.

Shabel, S.J., Proulx, C.D., Trias, A., Murphy, R.T., Malinow, R., 2013. Input to the lateral habenula from the basal ganglia is excitatory, aversive, and suppressed by serotonin. Neuron 74, 475–481. https://doi.org/10.1016/j.neuron.2012.02.037.

Shao, J., Gao, D.S., Liu, Y.H., Chen, S.P., Liu, N., Zhang, L., Zhou, X.Y., Xiao, Q., Wang, L. P., Hu, H.L., et al., 2022. Cav3.1-driven bursting firing in ventromedial hypothalamic neurons exerts dual control of anxiety-like behavior and energy expenditure. Mol. Psychiatr. 27, 2901–2913. https://doi.org/10.1038/s41380-022-01513-x.

Shreve, P.E., Uretsky, N.J., 1991. GABA and glutamate interact in the substantia innominata/lateral preoptic area to modulate locomotor activity. Pharmacol. Biochem. Behav. 38, 385–388. https://doi.org/10.1016/0091-3057(91)90296-E.

Thornhill, J., Halvorson, I., 1994. Activation of shivering and non-shivering thermogenesis by electrical stimulation of the lateral and medial preoptic areas. Brain Res. 656, 367–374. https://doi.org/10.1016/0006-8993(94)91481-8.

Tartt, A.N., Mariani, M.B., Hen, R., Mann, J.J., Boldrini, M., 2022. Dysregulation of adult hippocampal neuroplasticity in major depression: pathogenesis and therapeutic implications. Mol. Psychiatr. 27, 2689–2699. https://doi.org/10.1038/s41380-022-01520-y.

Walsh, J.J., Han, M.H., 2015. The heterogeneity of ventral tegmental area neurons: projection functions in a mood-related context. Neuroscience 282, 101–108. https://doi.org/10.1016/j.neuroscience.2014.06.006.

Waung, M.W., Maanumm, K.A., Cirino, T.J., Driscoll, J.R., O'Brien, C., Bryant, S.B., Mansourian, K.A., Morales, M., Barker, D.J., Margolis, E.B., 2022. A diencephalic circuit in rats for opioid analgesia but not positive reinforcement. Nat. Commun. 123, 764. https://doi.org/10.1038/s41467-022-28332-6.

Xia, G., Han, Y., Meng, F., He, Y., Srisai, D., Farias, M., Dang, M.H., Palmiter, R.D., Xu, Y., Wu, Q., 2021. Reciprocal control of obesity and anxiety-depressive disorder via a GABA and serotonin neural circuit. Mol. Psychiatr. 26, 2837–2853. https://doi.org/10.1038/s41380-021-01053-w.

Xu, L., Nan, J., Lan, Y., 2020. The nucleus accumbens: a common target in the comorbidity of depression and addiction. Front. Neural Circ. 14, 37. https://doi.org/10.3389/fncir.2020.00037.

Xu, X., Chen, R., Wang, L.B., Su, X.J., Xu, P.F., Liu, X.Q., et al., 2023. A glutamatergic DRN-VTA pathway modulates neuropathic pain and comorbid anhedonia-like behavior in mice. Nat. Commun. 14, 5124. https://doi.org/10.1038/s41467-023-40860-3.

Yang, Y., Wang, H., Hu, J., Hu, H.L., 2018. Lateral habenula in the pathophysiology of depression. Curr. Opin. Neurobiol. 48, 90–96. https://doi.org/10.1016/j.conb.2017.10.024.

Yamagata, T., Kahn, M.C., Prius-Mengual, J., Meijer, E., Šabanović, M., Guillaumin, M.C. C., van der Vinne, V., Huang, Y.G., McKillop, L.E., Jagannath, A., et al., 2021. The hypothalamic link between arousal and sleep homeostasis in mice. Proc. Natl. Acad. Sci. U.S.A. 118, e210158 https://doi.org/10.1073/pnas.2101580118.

Zhang, G.M., Wu, H.Y., Cui, W.Q., Peng, W., 2022. Multi-level variations of lateral habenula in depression: a comprehensive review of current evidence. https://doi.org/10.3389/fpsyt.2022.1043846.

Zheng, Z.W., Guo, C., Li, M., Yang, L., Liu, P.Y., Zhang, X.L., Liu, Y.Q., Guo, X.N., Cao, S. X., Dong, Y.Y., et al., 2022. Hypothalamus-habenula potentiation encodes chronic stress experience and drives depression onset. Neuron 110, 1400–1415. https://doi.org/10.1016/j.neuron.2022.01.011.

Zhong, P., Vickstrom, C.R., Liu, X.J., Hu, Y., Yu, L.K., Yu, H.G., Liu, Q.S., 2018. HCN2 channels in the ventral tegmental area regulate behavioural responses to chronic stress. Elife 7, e32420. https://doi.org/10.7554/eLife.32420.

Zhou, L., Liu, M.Z., Li, Q., Deng, J., Mu, D., Sun, Y.G., 2017. Organization of functional long-range circuits controlling the activity of serotonergic neurons in the dorsal raphe nucleus. Cell Rep. 18, 3018–3032. https://doi.org/10.1016/j.celrep.2017.02.077.